Holistic Atlases of Functional Networks and Interactions Reveal Reciprocal Organizational Architecture of Cortical Function

Jinglei Lv*, Xi Jiang*, Xiang Li*, Dajiang Zhu*, *Student Member, IEEE*, Shu Zhang, Shijie Zhao, Hanbo Chen, Tuo Zhang, Xintao Hu, Junwei Han, Jieping Ye, Lei Guo, Tianming Liu, *Senior Member, IEEE*

***Abstract*—For decades, it has been largely unknown to what extent multiple functional networks spatially overlap/interact with each other and jointly realize the total cortical function. Here, by developing novel sparse representation of whole-brain fMRI signals and by using the recently publicly released large-scale Human Connectome Project (HCP) high-quality fMRI data, we show that a number of reproducible and robust functional networks, including both task-evoked and resting state networks, are simultaneously distributed in distant neuroanatomic areas and substantially spatially overlapping with each other, thus forming an initial collection of holistic atlases of functional networks and interactions (HAFNI). More interestingly, the HAFNIs revealed two distinct patterns of highly overlapped regions and highly-specialized regions and exhibited that these two patterns of areas are reciprocally localized, revealing a novel organizational principle of cortical function.**

***Index Terms*— Cortical architecture, fMRI, interaction, brain networks.**

I. Introduction

Understanding the organizational architecture of cortical function has been of intense interest since the inception of human neuroscience. After decades of active research using in-vivo functional neuroimaging techniques such as fMRI [1], there has been mounting evidence [2]-[6] that the brain function emerges from and is realized by the interaction of multiple concurrent neural processes or networks, each of which is spatially distributed across specific structural substrate of neuroanatomical areas [7], [8]. However, it is still challenging to robustly and faithfully reconstruct concurrent functional networks from fMRI (either task fMRI (tfMRI) or resting state fMRI (rsfMRI)) data and quantitatively measure their network-level interactions. The critical lack of this key knowledge might be the underlying fundamental barrier to rigorously answering this long-standing debate in human neuroscience [9]: is the functional human brain architecture composed of a collection of highly specialized components, each responsible for a dedicated aspect of human function, or is the brain architecture more of a general-purpose machinery, each component of which involved in a wide range of functional processes?

Despite the remarkable successes and significant neuroscientific insights on fMRI analysis achieved by traditional GLM based subtraction approach [10], [11], it has been recognized and pointed out in the literature that spatially overlapping networks subserving different functions are possible to go unnoticed by the blocked subtraction paradigms and the associated analysis methods such as general linear model (GLM) [12], [13]. Meanwhile, from a human neuroscience perspective, it has been widely reported and argued that a variety of cortical regions and networks exhibit strong functional diversity and heterogeneity [2], [5], [6], [9], [14], [15], that is, a cortical region could participate in multiple functional domains/processes and a functional network might recruit various heterogeneous neuroanatomic areas. Therefore, it is unlikely that current subtraction-based tfMRI data analysis methods are sufficient to reconstruct concurrent spatially-overlapping functional networks and then to address the fundamental question of whether the functional brain architecture is composed of highly-specialized components, or is a general-purpose machinery, or is somewhere in-between.

Besides tfMRI for studying task-evoked cortical function, rsfMRI has arguably been another major neuroimaging technique to examine the intrinsic functional activities of the human brain [16]-[18]. Recently, a variety of computational methods, such as independent component analysis (ICA) [19], [20], normalized cut [21] or other clustering algorithms [22], have been employed to map resting state networks (RSNs) in healthy brains or neurological/psychiatric disorders, and many interesting results have been reported [17], [18], [23] [24].

Asterisk indicates that these authors contributed equally to this work.

J. Lv*, S. Zhao, and T. Zhang are with the School of Automation, Northwestern Polytechnical University, Xi'an, P. R. China, and with the Cortical Architecture Imaging and Discovery Lab, Department of Computer Science and Bioimaging Research Center, The University of Georgia, Athens, GA, 30602 USA (e-mail: lvjinglei@gmail.com ; shijiezhao666@gmail.com; zhangtuo.npu@gmail.com;).

X. Jiang*, X. Li*, D. Zhu*, S. Zhang, H. Chen are with the Cortical Architecture Imaging and Discovery Lab, Department of Computer Science and Bioimaging Research Center, The University of Georgia, Athens, GA, 30602 USA (e-mail: superjx2318@gmail.com; xiangli@uga.edu ; dajiang.zhu@gmail.com;shuzhang1989@gmail.com;cojoc.chen@gmail.com).

X. Hu, J. Han, L. Guo are with the School of Automation, Northwestern Polytechnical University, Xi'an, P. R. China (e-mail: xintao.hu@gmail.com; junweihan2010@gmail.com; guolei.npu@gmail.com).

J. Ye is with Department of Computer Science and Engineering, Arizona State University, Tempe, AZ, USA. (e-mail: jieping.ye@asu.edu).

T. Liu is with the Cortical Architecture Imaging and Discovery Lab, Department of Computer Science and Bioimaging Research Center, The University of Georgia, Athens, GA, 30602 USA (corresponding author; phone: (706) 542-3478; e-mail: tianming.liu@gmail.com).

However, there has been limited knowledge about to what extent the reconstructed RSNs spatially overlap with each other and jointly realize resting state brain function. In addition, there has been increasing interest in examining the relationship or interaction between task-evoked networks and intrinsic RSNs in the literature [27].

In order to address the abovementioned fundamental questions, in this work, we developed a novel computational framework of sparse representations of whole-brain fMRI signals and applied it on the recently publicly released large-scale Human Connectome Project (HCP) tfMRI data (Q1 release) [28]. The basic idea of our computational framework is to aggregate all of hundreds of thousands of tfMRI or rsfMRI signals within the whole brain of one subject into a big data matrix, which is subsequently factorized into an over-complete dictionary basis matrix (represented by the panel (I) of Fig.1) and a reference weight matrix (represented by the panel (II) of Fig.1) via an effective online dictionary learning algorithm [29, 30]. Then, the time series of each over-complete basis dictionary represents the functional BOLD (blood-oxygen-level dependent) activities of a brain network (the white curves in the panel (II) of Fig.1) and its corresponding reference weight vector stands for the spatial map of this brain network (the volume images in the panel (II) of Fig.1). A particularly important characteristic of this framework is that the decomposed reference weight matrix naturally reveals the spatial overlap/interaction patterns among reconstructed brain networks (illustrated in Supplemental Fig.1). Experimental results on the HCP datasets have shown that these well-characterized functional networks are reproducible across different tasks and individual brains and exhibit substantial spatial overlaps with each other (Supplemental Fig.1i-1o), thus forming an initial collection of holistic atlases of functional networks and interactions (HAFNI). More interestingly, these HAFNIs revealed two distinct patterns of highly heterogeneous (highly overlapped) regions and highly-specialized (task-evoked) regions in tfMRI data and showed that these two patterns of areas are reciprocally localized.

II. Materials and Methods

A. Dataset and preprocessing

The primary goals of the HCP tfMRI datasets were to identify as many core functional nodes in the brain as possible that can be correlated to structural and functional connectomes and behavior measurements [28]. To achieve this objective, a broad battery of tasks were adopted or designed to identify core node locations in as a wide range of neural systems as feasible within realistic time constraints. Thus the HCP tfMRI dataset can be considered as a systematic and comprehensive mapping of connectome-scale functional networks and core nodes over a large population in the literature so far. The specifics of seven tasks are briefed in supplemental materials.

In the first Q1 release of HCP fMRI dataset, 77 participants are scanned. Specifically, 58 are female and 19 are male, 3 are between the ages of 22–25, 27 are between the ages of 26–30, and 47 are between the ages of 31–35. In the publicly released dataset, only 68 subjects are available. So our experiments are based on the 7 tasks and 1 resting state fMRI data of 68 subjects.

The acquisition parameters of tfMRI data are as follows: 90×104 matrix, 220mm FOV, 72 slices, TR=0.72s, TE=33.1ms, flip angle = 52°, BW =2290 Hz/Px, in-plane FOV = 208 × 180 mm, 2.0 mm isotropic voxels [28]. For tfMRI images, the preprocessing pipelines included skull removal, motion correction, slice time correction, spatial smoothing, global drift removal (high-pass filtering). All of these steps are implemented by FSL FEAT. For results comparison, the GLM-based activation is also performed individually and group-wisely using FSL FEAT. Task designs are convoluted with the Double Gamma haemodynamic response function and set as regressors of GLM. The contrast based statistical parametric mapping was carried out with T-test and $p<0.05$ (with cluster correction) is used to reject false positive. Multi-level z-scores are used to map multi-scale activations. In the group level, the statistical parametric mapping is carried out with mixed-effect model embedded in the FSL FEAT tool. For the rsfMRI data, the acquisition parameters were as follows: 2×2×2 mm spatial resolution, 0.72 s temporal resolution and 1200 time points. The pre-processing of rsfMRI data also include skull removal, motion correction, slice time correction, spatial smoothing. More detailed about rsfMRI data acquisition and preprocessing are referred to literature report [31].

B. Dictionary Learning and Sparse Coding

The computational framework of dictionary learning and sparse coding of whole-brain fMRI signals is summarized in Supplemental Fig.10. Specifically, first, for each single subject's brain in one task scan, we extract tfMRI signals on all voxels of the whole brain. Then, after normalizing the signals to zero mean and standard deviation of 1, they are arranged into a big signal data matrix $X \epsilon \mathbb{R}^{t \times n}$ (Supplemental Fig.10a), where n columns are fMRI signals from n voxels and t is the fMRI volume number (or time points). By using a publicly available effective online dictionary learning and sparse coding method [30], each fMRI signal vector in X is modeled as a linear combination of atoms of a learned basis dictionary D (Supplemental Figs.10b-10c), i.e., $x_i = D \times \alpha_i$ and $X=D \times \alpha$, where α is the coefficient weight matrix for sparse representation and each column α_i is the corresponding coefficient vector for x_i.

At the same time, we map each row in the α matrix back to the brain volume and examine their spatial distribution patterns, through which functional network components are characterized on brain volumes, as shown by the red and yellow areas in Supplemental Fig.10c. At the conceptual level, the sparse representation framework in Supplemental Fig.10 can achieve both compact high-fidelity representation of the whole-brain fMRI signals (Supplemental Fig.10b) and effective extraction of meaningful patterns (Supplemental Fig.10c) [29], [30], [32]-[35]. In comparison with previous works of sparse representation of fMRI signals [36]-[39], the major novelty here is that our framework holistically considers

the whole-brain tfMRI signals by using a big-data strategy and aims to infer a comprehensive collection of functional networks concurrently, based on which their spatial and temporal characteristics can be quantitatively described and modeled.

In this framework, we aim to learn a meaningful and over-complete dictionary of functional bases $D\epsilon\mathbb{R}^{t\times m}$ ($m>t$, $m<<n$) [30] for the sparse representation of X. For the task-based fMRI signal set $X=[x_1, x_2, \dots x_n]\epsilon\mathbb{R}^{t\times n}$, the empirical cost function is summarized in Eq.(1) by considering the average loss of regression of n signals.

$$f_n(D) \triangleq \frac{1}{n}\sum_{i=1}^{n}\ell(x_i, D) \tag{1}$$

With the aim of sparse representation using D, the loss function is defined in Eq.(2) with a ℓ_1 regularization that yields a sparse resolution of α_i, and here λ is a regularization parameter to trade-off the regression residual and sparsity level.

$$\ell(x_i, D) \triangleq \min_{\alpha_i\epsilon\mathbb{R}^m}\frac{1}{2}||x_i - D\alpha_i||_2^2 + \lambda||\alpha_i||_1 \tag{2}$$

As we mainly focus on the fluctuation shapes of basis fMRI activities and aim to prevent D from arbitrarily large values, the columns $d_1, d_2, \dots \dots d_m$ are constrained by Eq.(3).

$$C \triangleq \left\{D\epsilon\mathbb{R}^{t\times m} \quad s.t. \quad \forall j = 1, \dots m, \qquad d_j^T d_j \le 1\right\} \tag{3}$$

$$\min_{D\epsilon C, \alpha\epsilon\mathbb{R}^{m\times n}}\frac{1}{2}||X - D\alpha||_F^2 + \lambda||\alpha||_{1,1} \tag{4}$$

In brief, the problem of dictionary learning can be rewritten as a matrix factorization problem in Eq.(4) [40], and we use the effective online dictionary learning method [30] to derive the atomic basis dictionary for sparse representation of whole-brain fMRI signals. Here, we employ the same assumption as previous studies [25], [36]-[39] that the components of each voxel's fMRI signal are sparse and the neural integration of those components is linear.

One common use of sparse representation of signals with limited number of atoms from a learned dictionary is to de-noise. For our application, with the sparse representation, the relevant basis components of fMRI activities will be selected and linearly combined to represent the original fMRI signals. With the same regularization in Eq.(4), we perform sparse coding of the signal matrix using the fixed dictionary matrix D in order to learn an optimized α matrix for spare representation as shown in Eq.(5).

$$\min_{\alpha_i\epsilon\mathbb{R}^m}\frac{1}{2}||x_i - D\alpha_i||_2^2 + \lambda||\alpha_i||_1 \tag{5}$$

Eventually, the fMRI signal matrix from a single subject's whole brain will be represented by a learned dictionary matrix and a sparse coefficient matrix (Supplemental Fig.10). Here, each column of the α matrix contains the sparse weights when interpreting each fMRI signal with the atomic basis signals in the dictionary. Meanwhile, each row of the α matrix represents the spatial volumetric distributions that have references to certain dictionary atoms. With these decomposed dictionary components and their weight coefficient parameters across the whole brain for each subject, our major task is to characterize and interpret them within a neuroscience context. In particular, the sparse representation and dictionary learning of whole-brain fMRI signals (Supplemental Fig.10) are performed for each individual brain separately and thus the spatial and temporal correspondences of those characterized dictionary components, or functional networks, across a group of subjects will be another major objective, as detailed in the next section.

One major advantage of the sparse coding strategy is that the sparsity or scale of spatial regions in each component can be controlled and concentrated by the regularization of λ, but based on current knowledge in machine learning field there is no golden criteria about defining λ. So we empirically employed the sparsity of λ=1.5 based on the criterion of group-wise consistency of derived HAFNI components. Our experimental results show that based on the results in supplemental material Section I.B, the spatial maps and temporal patterns are not so sensitive to λ when it alternates in a certain level such as 1.0 to 2.0. Another critical parameter is the dictionary size. After exploring the dictionary size from 100 to 600 in the supplemental materials, it is clear that the meaningful networks changes very slightly with alternation of dictionary size. Finally, the dictionary size in this paper is experimentally set as 400.

C. HAFNI Networks Identification

We have applied the above dictionary learning and sparse representation methods on the publicly available HCP release tfMRI datasets. Specifically, for each single individual, seven scans of task fMRI data and one scan of resting state fMRI data were acquired and preprocessed separately. The HAFNI pipeline was applied to each scan of each subject independently. So all analysis results in the following sections are based on the single scan of each subject. Then the following procedures of both quantitative measurements and visual examination of the spatial and temporal pattern of the obtained functional networks (dictionary atoms) were applied to identify networks that can be well-characterized and interpreted by existing brain science knowledge. Specifically, in tfMRI data, some of these networks have similar spatial and temporal patterns as the activation detection results (contrast maps) by using general linear model (GLM), as shown in Supplemental Figs.2a-2j (10 randomly selected subjects). As the time series of each basis dictionary is considered as a functional network component, we aim to characterize and model as many network components as possible (as already illustrated in Fig.1), and to seek their correspondences across individual brains. To achieve this goal, we not only compared each dictionary atom's temporal shape pattern (white curve in image (III) of each panel in Fig.2a) with the task paradigm curve (red curve in image (III) of each panel in Fig.2a), each red curve for one separate task contrast), but also examined the similarity between the dictionary atom's spatial reference weight map (image (I) in each panel in Fig.2a) and the activation map (image (II) in each panel in Fig.2a) obtained by traditional GLM method. Specifically, we defined the spatial overlap rate (Eq.(6)) to

measure the similarity of the two maps. Our rationale here is that each identified and characterized HAFNI component should exhibit both high temporal similarity with the task paradigm and high spatial similarity with the GLM-derived activation map. In addition, we evaluated the group-wise consistency of the dictionary atom's spatial reference weight maps across all of the HCP subjects, as shown in Fig.2b as an example, and only those most group-wise consistent dictionary atoms are considered as HAFNI components.

In this work, we aim to construct an initial set of functional atlases (called holistic atlases of functional networks and interactions (HAFNI)) characterizing consistent functional brain networks across HCP subjects in all seven tfMRI datasets. More specifically, in tfMRI data, for each single contrast map of an individual subject obtained by GLM, we first applied 7 levels of z-score thresholds (1.0-4.0 stepped by 0.5) on it. Note that selecting multi-level of threshold is because there is no golden criterion for significance of activation detection, and we need to find a suitable match between the activation and the component network. Afterwards we picked up 10 candidate networks with higher spatial similarity with that contrast map of specific threshold and temporal correlation with task contrast design, as shown in our website:http://cobweb.cs.uga.edu/~hafni/HCPTask_ReportThresholded/HTML/. The spatial similarity is defined by the overlap rate R between spatial pattern of the network (A) and the spatial pattern of the contrast maps serving as the template (T):

$$R(A,T) = \frac{|A \cap T|}{|T|} \quad (6)$$

A team of experts then quantitatively and qualitatively identified the best matches between HAFNI networks and GLM contrast maps. Seven experts were involved in the network identification. They searched network candidates separately, while the final results are based on the agreement reached by a voting procedure. For example, for the contrast 5 of the motor task, the GLM spatial maps and HAFNI candidate components are shown in the link http://cobweb.cs.uga.edu/~hafni/HCPTask_ReportThresholded/HTML/Report_sub_11_MOTOR.html#MOTOR_cope_05. The group-wise GLM activation and individual activations with 7 level thresholds are shown in the first 3 rows. For each level of threshold, there are 10 candidate HAFNI components arranged in the same column. Note that each candidate is visualized with the spatial map and temporal curve overlaid with the contrast design. Our experts first selected an appropriate level of threshold for the GLM activation, and then the final HAFNI component was selected based on both the similarity with spatial activation map and the correlation of temporal curve and task design. Note that both spatial patterns and temporal time series shapes are taken into consideration as they provide complementary information regarding the neuroanatomic distributions and temporal dynamics of functional activities. Both sources of information can contribute to the identification and characterization of those brain networks. In this example, the GLM threshold is selected as 4.0 for reasonable patterns, and the HAFNI network of the subject corresponding to the contrast is selected as component #256 (out of 400 candidate ones) with both high spatial similarity with activation pattern and temporal correlation with contrast design. After summarizing the identification results from all 7 tasks across 68 subjects, there are totally 23 consistent task-evoked functional networks identified, constituting the current initial version of HAFNI. The complete list of the final HAFNI networks vs. GLM contrast maps can be accessed on our website at: http://hafni.cs.uga.edu/finalizednetworks_Task.html.

For resting state networks (RSNs) identification in seven tfMRI datasets and one rsfMRI dataset across all 68 HCP subjects, since the temporal characteristics of RSNs have not been fully understood or quantitatively described, we adopted the spatial similarity measurement defined in Eq.(6) to identify meaningful RSNs. In this work, we adopted the ten well-defined RSN templates provided in the literature [41]. For each tfMRI/rsfMRI data of each subject, we identified the component (dictionary atom) with the highest spatial similarity with each specific RSN template. Then a team of six experts quantitatively and qualitatively compared each identified component's spatial reference weight map with the corresponding RSN template in each task/resting state fMRI data of each subject. If the mean spatial similarity value of the identified component with the corresponding RSN template across all 68 subjects is less than 0.2 in any of the tfMRI/rsfMRI data, this RSN component will be discarded. For example, in the emotion task data of subject 1, the identified components with the corresponding RSN templates are shown in http://hafni.cs.uga.edu/HCPResting_Report/Report_Resting_State_01.html#EMOTION. After quantitative and qualitative inspection by the experts, RSN #5 representing the cerebellum was discarded for all 68 subjects in the tfMRI/rsfMRI data. Finally, nine meaningful RSNs were successfully identified in all of the seven tfMRI datasets and one rsfMRI dataset of all subjects. Supplemental Figs.4a-4j show the nine identified RSNs via HAFNI in all seven tfMRI datasets and one rsfMRI dataset of 10 randomly selected subjects. The complete list of the final HAFNI RSNs are at: http://hafni.cs.uga.edu/finalizednetworks_Resting.html.

We further examined the possible functional identities/roles of these HAFNI RSNs based on existing brain science knowledge and literature reports. Specifically, RSNs #1, #2 and #3 are all located in the visual cortex, and contain medial occipital pole (BA 17) and lateral visual areas (BAs 18/19), respectively. RSN #4, widely known as the 'default mode network' (DMN) [42] includes the medial prefrontal gyrus (BAs 9/10/11), anterior (BAs 12/32)/posterior (BA 29) cingulate cortex, and bilateral supramarginal gyrus (BA 39). RSN #5 mainly includes pre- and post-central gyrus (BAs 1/2/3/4), and the supplementary motor area (SMA) (BA 6), and is known as the sensorimotor network. RSN #6 is known as the auditory network, including the Heschl's gyrus, posterior insular cortex and lateral superior temporal gyrus. RSN #7 is considered as the executive control network, including anterior

cingulate and paracingulate regions. Finally, RSNs #8 and #9 have strong lateralization in the right (RSN #9) and left (RSN #10) hemispheres, containing the middle frontal and orbital (BAs 6/9/10) and superior parietal areas (BAs 7/40).

Moreover, for comparison purpose, we performed independent component analysis (ICA) on the whole-brain rsfMRI data of each single HCP subject using FSL MELODIC tool [19] as an independent source to evaluate the identified HAFNI RSNs from tfMRI data. Specifically, we set ICA dimensionality as 100, which has been proven appropriate and effective in the literature. We adopted the same spatial overlap rate metric for identifying corresponding ICA components. The ICA component with the highest spatial overlap rate with a specific RSN template [41] was determined as the specific RSN in the rsfMRI data of a specific subject.

It is essential to mention that our HAFNI framework is independent from the GLM-based fMRI activation detection and ICA-based resting state network identification. Without effective interpretation of the hundreds of networks generated by HAFNI, the GLM activation and ICA results are employed to identify meaningful networks in HAFNI. On the other hand, further comparison of spatial patterns and temporal characteristics across these methods is a reasonable verification of the effectiveness of our HAFNI method.

D. Spatial Overlap Patterns among Task-evoked and Resting State Functional Networks

To quantitatively measure the overlap patterns, we adopted the following scheme to define the spatial overlap rate (OR):

$$OR_i = \frac{R_i}{R_{involved}} \tag{7}$$

In the above formula, *i* represents the number of overlap components in a specific situation and it is variable under different conditions (task contrast, HAFNI RSNs or their combination). For instance, in motor task, there are 5 contrasts with which we can identify the corresponding HAFNI components. We calculated the percentage of the voxels simultaneously recruited in *i* components to those voxels involved in at least one component. In this case, *i* changes from 2 to 5. Similarly, in the calculation of OR in HAFNI RSNs, *i* changes from 2 to 9. It should be noted that when we estimate OR between task-evoked HAFNI components and HAFNI RSNs, R_i are the voxels belonging to both of them at the same time, and $R_{involved}$ represents the voxels involved at least one task contrast or one HAFNI RSN.

The highly-heterogeneous region (HHR) region is defined by the number of networks/components involved within the region. Specifically, an HHR region is composed of a collection of voxels that:

$$\text{HHR} = \forall voxel\ v_i\ s.t. \|\alpha_i\|_0 > Threshold \tag{8}$$

Thus, any voxel on the cerebral cortex with the number of non-zero elements (i.e., the number of involved networks) in its corresponding column in coefficient matrix $\|\alpha_i\|_0$ greater than a pre-defined threshold would be included in the HHR. As in this work the dictionary size was experimentally set as 400 (please see the below section for more details), $\|\alpha_i\|_0$ is in the range of 0 to 400. The threshold is defined by the number of non-zero elements in the top 20% percentile across all voxels, so that we would obtain similarly-sized HHR for different fMRI datasets. The rationale for using a single uniform threshold in defining the HHR is based on our observation that the values of $\|\alpha\|_0$ across voxels are typically normally distributed in all tfMRI datasets with similar mean and standard deviation (please see Supplemental Fig.5). We have examined the effect of threshold by performing the same analysis using different thresholds and have obtained similar conclusions (please see Supplemental Table VIII). Also, we define the highly-specialized regions (HSR) as voxels that are involved in task-related networks.

III. RESULTS

A. Group-wise Consistent Task-evoked Functional Networks

In total, we identified and confirmed 5, 3, 2, 2, 2, 3 and 6 group-wise consistent task-evoked networks, or called HAFNI components here, for motor (M1-M5 in Fig.2a), emotion (E1-E3 in Fig.2a), gambling (G1-G2 in Fig.2a), language (L1-L2 in Fig.2a), relational (R1-R2 in Fig.2a), social (S1-S3 in Fig.2a), and working memory (WM) (W1-W6 in Fig.2a) networks, respectively. These networks are correlated to specific task performance, e.g., M1 is for right hand movement, M2 is for tongue movement, M3 is for global motion task, M4 is for left hand movement, E1 is for emotional faces stimulus, E2 is for simple shape stimulus, W1 is for 2-back memory task, and W2 is for 0-back memory task. Additional details about the network description are referred to Supplemental Table XIII. In particular, these 23 HAFNI components are reproducible and consistent across all of the HCP subjects we examined, as shown in Supplemental Figs.2a-2j and in the visualizations on our website: http://hafni.cs.uga.edu/finalizednetworks_Task.html. In Figs.2b-2d and Supplemental Figs.3a-3g, the averaged spatial map of each HAFNI component across all subjects is shown and compared with the corresponding group-wise GLM-derived activation map. It is evident that the averaged HAFNI components are similar to the group-wise GLM-derived maps. Quantitatively, Supplemental Table I provides the spatial overlap rates of HAFNI components and GLM-derived activation maps for 20 randomly selected individuals, and the average of spatial overlap rate is 0.47. In addition, Supplemental Table II shows the Pearson's correlations of the HAFNI component's temporal time series and the task paradigm curves for the same 20 subjects, and the average correlation is 0.39. These results demonstrated that the dictionary learning method and the HAFNI identification procedure can effectively uncover meaningful task-evoked functional networks, and can serve as a novel, alternative approach to detecting traditionally-conceived task-based activations. In Table I, the individual variation between HAFNI and GLM is substantial, the reason of which is attributed to the following two aspects. 1) The regression strategy in GLM that only employ limited regressors might not be sufficient in dealing with the diversity of hemodynamic behaviors and the

heterogeneous brain regions, so that the results from the GLM is fragile and is different from the HAFNI results. 2) The GLM method might not be capable of determining task related activations in the areas with complicated signals, while the HAFNI method can decompose task related components in these areas.

Importantly, a fundamental difference between the HAFNIs and GLM-based activation maps is that the HAFNI components are simultaneously derived from the optimally de-composed fMRI signals based on the sparse representation of whole-brain data (as illustrated in Fig.1), while the GLM-based maps were obtained from individual fMRI signals based on separate model-driven subtraction procedures. For instance, the five HAFNI components (M1-M5 in Fig.2a) in the motor tfMRI data can be effectively and robustly derived by characterizing the most relevant atoms from a library of candidate dictionaries (the panel (I) of Fig.1), which can maximally account for the whole-brain fMRI signals. In contrast, the model-driven GLM procedure is applied on individual fMRI signals whose compositions could be contributed from multiple functional processes or networks. As a consequence, the GLM has difficulty in reconstructing concurrent, interacting functional networks, and thus other spatially overlapping networks with different temporal curves (such as the RSNs in the panel (II) of Fig.1) other than the task paradigm will be essentially unnoticed [12] [13]. Also, the experimental comparison between HAFNI method and GLM method based on synthesized data in Supplemental Methods. C (Performance on Synthetic Data) provides additional sound evidence that the HAFNI method performs better in reconstructing concurrent interacting function networks. In the synthetic experiments, the HAFNI method exhibits clear advantages in reconstructing temporal response of networks and is superior in the sensitivity, precision and false discovery rate of reconstructed spatial maps of concurrent brain networks. Therefore, it is appropriate and feasible to employ the HAFNI components, instead of the GLM-derived maps, to explore the question of how the total cortical function is realized by the interaction of multiple concurrent neural processes or networks [2]-[8].

B. Group-wise Consistent Resting-state Functional Networks

We went through all of the decomposed dictionary components (e.g., the panel (I) of Fig.1) and identified nine reproducible and consistent RSNs in all of the seven tfMRI datasets across all of the HCP subjects. Fig.3a shows the nine RSNs (nine rows) in these seven tasks (the first seven columns) for one exemplar subject. Meanwhile, for comparison purpose, the corresponding RSNs identified by both of the dictionary learning method and the independent component analysis (ICA) [19] method from rsfMRI data are shown in the eighth and ninth columns in Fig.3a. It is evident that all of the nine RSNs derived from either tfMRI or rsfMRI data are consistent with the template [41], and thus are called HAFNI RSNs here. Particularly, the nine HAFNI RSNs can be robustly reconstructed across individuals, as shown in Fig.3c, in Supplemental Figs.4a-4j, and on our website: http://hafni.cs.uga.edu/finalizednetworks_Resting.html. In addition, the averaged HAFNI RSNs maps across all HCP subjects are shown in Fig.3b, and quantitatively the mean spatial overlap rate of nine HAFNI RSNs is as high as 0.59, as detailed in Supplemental Table III. Supplemental Table IV shows the spatial overlap rates of nine HAFNI RSNs across all HCP subjects. These results demonstrated that no matter what the task is, the nine RSNs can be robustly reconstructed and reproduced by the sparse representation and HAFNI identification method. Thus, the identification of these HAFNI RSNs lays out a solid foundation to explore the question of to what extent the RSNs spatially overlap and interact with task-evoked functional networks obtained in the above section.

For comparison purpose, Fig.3a (the ninth column) shows the identified RSNs via ICA in the rsfMRI data of the same subject. Supplemental Table V details the mean overlap rates of nine HAFNI RSNs in rsfMRI data and those by ICA across all subjects. The mean overlap rate is 0.56±0.07 for HAFNI RSNs, and is 0.55±0.09 for ICA. Both qualitative (Fig.3a and Supplemental Figs.4a-4j) and quantitative (Supplemental Table V) results indicate that the HAFNI method can consistently and reliably identify RSNs in rsfMRI data too, compared with the widely-used ICA method. However, a critical difference between the dictionary learning/sparse representation method and the ICA method is that ICA explicitly assumes the independence of fMRI signals among different components, while the sparse representation does not. Essentially, multiple functional processes or network components (illustrated in Supplemental Fig.1) could be spatially overlapping and interacting with each other in resting state or under task performance [2], [5], [6], [9], [14], [15], and it has been pointed out in the literature that fMRI signals are not necessarily independent [25], [26]. Therefore, it is more appropriate and feasible to employ the HAFNI RSNs, instead of the ICA-derived components, to explore the question of how the total cortical function is realized by the interaction of multiple concurrent neural processes or networks [2]-[8]. In this work, the 9 HAFNI RSNs and other 23 task-evoked HAFNI components (in the above section) are simultaneously derived from the same procedure of matrix factorization of whole-brain fMRI signals (Fig.1), which naturally represents the spatial overlap and functional interaction patterns among the initial collection of holistic brain networks and provides an enabling platform to explore functional cortical architectures.

C. Spatial Overlap Patterns among HAFNI Components

Based on the above task-evoked HAFNIs and HAFNI RSNs, we examined their spatial overlaps with each other, including overlaps among multiple contrast-evoked HAFNIss within the same task and overlaps between task-evoked HAFNIs and HAFNI RSNs. Specifically, Fig.4a visualized the overlap patterns in all seven tasks for one randomly selected subject. From Fig.4a, we can clearly see the substantial overlaps not only among different contrast-evoked components but also between task-evoked HAFNIs and HAFNI RSNs. For example, for the motor task (the first column of Fig.4a), there exist multiple regions that are simultaneously recruited by multiple

task contrasts and motor/auditory RSNs. In addition, the extent of spatial overlaps is quantitatively measured by the number of HAFNI components that each brain region is involved in and is color-coded in Fig.4b. The widespread red regions in Fig.4b depict those highly overlapped cortical areas, revealing the functional interaction patterns of the well-characterized HAFNI components in seven tasks.

Quantitatively, the overall spatial overlap rate (OR) (defined in Eq.(7)) result is summarized in Supplemental Table VI, which is interpreted as follows. First, spatial overlap between/among different contrast-evoked components is quite common and widespread. For instance, the average spatial overlap rate for two contrast-evoked components in motor, emotion, gambling, relational, social and working memory tasks are 20.6%, 17.7%, 23.3%, 29.4%, 25.3%, and 20.6%, respectively. These results demonstrated that contrast-evoked network components within the same task are substantially overlapped in the spatial domain, suggesting their functional interactions. Notably, the ORs among different contrasts have considerable variation across seven tasks. For example, the ORs for language and relational tasks are of 0.8% and 29.4%, respectively. For comparison, we have also calculated the overlap rate between the activation detection (activated-baseline) results obtained by the general linear model (GLM) in each task, which are summarized in Supplemental Table XII. As shown in the table, the overlap rate between the activation detection results from GLM follows the same trend as in the contrast-evoked components from HAFNI, yet with a substantially lower value. The explanation for the higher spatial overlapping rate of HAFNI results is the fact that the data-driven, automatically identified components obtained by HAFNI are able to include regions with more complicated functional characteristics, while those regions would more frequently serve for the functional interaction thus tend to be recruited in multiple contrasts.

Second, spatial overlap between/among different HAFNI RSNs is also quite common and widespread, as shown in Fig.4 and Supplemental Table VI. Notably, compared to task contrasts, HAFNI RSNs have relatively more consistent overlap patterns. As shown in Supplemental Table VI, the ORs of two HAFNI RSNs in seven tasks range from 9.3% to 15.4%, and the ORs of three HAFNI RSNs range from 0.7% to 2.2%. The spatial distributions of these overlaps in one subject are visualized on the cortical surface in the second rows of Fig.4a and Fig.4b. It is interesting that these RSNs overlap patterns are reasonably stable and reproducible across a variety of tasks, suggesting the reliability of RSNs-related organizational architecture of the human brain.

Third, there are considerable spatial overlaps between task-evoked HAFNIs and HAFNI RSNs, as shown in the third rows of Figs.4a-4b and Supplemental Table VI. The average OR between task contrast-evoked components and HAFNI RSNs is 9.7%, and in particular, this OR value in working memory even reaches 20.0%. More quantitative details for each task are in the last row of Supplemental Table VI. In general, these results quantitatively demonstrated an interesting phenomenon: RSNs exhibited substantial spatial overlaps/interactions with task-evoked networks during task performance.

D. Reciprocal Localization of Highly-Heterogeneous Region and Highly-specialized Regions

The previous sections have revealed the common and widespread spatial overlaps among 32 well-characterized HAFNI components. In this section, we aim to investigate other un-characterized network components and their composition patterns over the cerebral cortex. Our extensive observations of such network composition patterns suggest that there are two distinct patterns for cortical regions, one is involved in multiple functional networks and is thus named “highly-heterogeneous region (HHR)”, and another is mainly responding to the task and therefore is named “highly-specialized regions (HSR)”. A visual illustration of the HHR along with HSR obtained by GLM-based activation detection is shown in Fig.5. It can be seen that HHR regions (red) are spatially distributed around the whole cortex, with very small overlaps with the HSR regions (blue). Such observation is quite consistent throughout all of the seven tasks and across all subjects, as shown in the additional cases in Supplemental Figs.6-7. Quantitatively, the overlap rates between the HHR and HSR regions of 20 randomly selected subjects are summarized in Supplemental Table VII. It is evident that the overlap rates are quite small (mostly <5%). In addition, the difference between HHRs and HSRs can be revealed by their temporal characteristics. For instance, while the mean tfMRI time series across all the voxels of the HSR region (Fig.5d1) is highly correlated with the task paradigm, as expected, the mean tfMRI time series of HHR region (Fig.5f1) is much more complex. Moreover, we have examined the component histogram of the HSR region and the HHR region by summing up the number of non-zero elements of each component in each voxel within the given region, and then normalized them to the sum of 1. The histograms of the HSR region and HHR region of a randomly selected subject during motor task are shown in Fig.5c and Fig.5e. It can be seen that the component histogram of HSR region is highly concentrated on certain components. Interestingly, the top two components in the histogram are exactly the components that had been identified as task-evoked HAFNI networks (M1 and M3), indicating the component-wise correspondence between GLM activation detections and HAFNI results.

On the contrary, the component histogram of HHR is more evenly-distributed and composed of various types of components. In particular, there are RSNs highly involved in the HHR, including RSN 3 and RSN 7 (highlighted in the figure), with RSN 7 being among the highest active networks in the region. As expected, task-evoked HAFNI components like M1 and M3 also have a relatively high percentage in the histogram, showing that certain parts of HHR participate in those tasks as well. In addition, such heterogeneities in the component histograms in HHRs are confirmed and illustrated at the individual voxel level in Supplemental Fig.8, which shows much more complexity and heterogeneity in the component composition of the voxels in HHR than those in the voxels of HSR. Further, we have investigated the overlap of the

activation detection results obtained by GLM across multiple tasks, by obtaining the intersections of the contrast maps (task-baseline). It was found that there exist certain regions in the brain that would be involved in the contrast maps from different tasks using GLM. A spatial comparison of those cross-task GLM result regions with the frequent-HSR shows that they are largely in accordance (average similarity of 65%), which is reasonable as HSR is mainly composed of the task-evoked HAFNI networks as shown in the analysis above.

Therefore, due to the complex network composition, those HHR regions could not be identified solely by their temporal time series pattern and could only be characterized by their network compositions like Fig.5e. Quantitatively, we used the histogram entropy to quantify the difference in the complexity of the component histogram between HSR and HHR. The results shows that there is a significant difference between those two regions regarding the histogram entropy ($p<0.01$), and the detailed quantifications are shown in Supplemental Table IX. In addition, we have defined the histogram concentration as:

$$\text{Concentration}(H) = \sum_{i=1}^{5} \max(H)_i \quad (9)$$

which is the summed percentage of the top 5 components in the histogram. A higher summed percentage value indicates that the distribution of the histogram is more concentrated on several dominant components. The concentration values of 20 randomly selected subjects are shown in Supplemental Table VII. Again, there is a significant difference between HSR and HHR ($p<0.01$), quantitatively verifying the histogram difference between HSR and HHR observed in Fig.5. The above results demonstrated that HHRs and HSRs are reciprocally located on the cerebral cortex within a specific cognitive or functional task.

Moreover, we examined frequent HHRs (F-HHR) and frequent HSRs (F-HSR) across all of the 7 tasks for each individual brain. Specifically, if an HHR or HSR region appears at least 4 times across 7 tasks (any possible combination from 7 tasks), it is considered as an F-HHR or F-HSR. Thus, to some extent, an F-HHR region can be considered as the multiple-demand (MD) area of the brain [2], [4], while an F-HSR region can be considered as a demand-specific (DS) area [2]. It is interesting that those two types of F-HHR and F-HSR areas are also reciprocally distributed and widespread across the cerebral cortex, as shown in Fig.6 and Supplemental Fig.9. In short, our results suggest that the functional cortical architecture is composed of a reciprocal combination of frequent highly-specialized regions and frequent highly-heterogeneous region across different types of cognitive or functional tasks.

IV. Discussion and Conclusion

In this work, we decomposed fMRI signals into linear combinations of multiple components based on sparse representation of whole-brain fMRI signals. This novel data-driven strategy naturally accounts for that a brain region might be involved in multiple functional processes [2], [5], [6], [9], [14], [15] and thus its fMRI signal is composed of various components. Experimental results have demonstrated that this novel strategy can effectively and robustly reconstruct concurrent functional networks, including both task-evoked HAFNIs and HAFNI RSNs, which can be reproduced across individuals. However, despite that we have characterized and interpreted 32 HAFNI components in spatial and/or temporal domains, there are still many other components remaining to be characterized and interpreted. These networks could be unknown networks or just noise networks, which need effective methodology to explore in the future. The 32 HAFNI components reported here is just a start point towards holistic atlases of functional networks in the future. Notably, the identification of HAFNI components heavily relied on experts' visual inspection in this work. In the future, novel methods should be developed to automatically identify consistent and reproducible HAFNI components across individuals and populations, as well as characterizing artefacts components.

GLM-based activation detection and ICA-based clustering have been arguably the dominant methods in tfMRI and rsfMRI data analyses, respectively. In this work, an alternative novel sparse representation and dictionary learning methodology is proposed to effectively infer the spatial overlap/interaction patterns among those brain networks. Experimental results have revealed the common and widespread spatial overlaps within and among both task-evoked and resting state networks, and particularly discovered the reciprocal localization of HHRs and HSRs. In the future, the regularity and variability of such reciprocal localization patterns of HHRs and HSRs should be examined across individual brains and be correlated with structural neuroimaging data. In addition, extensive quantitative studies should be performed to compare the sparse representation method with the GLM and ICA methods [19], [24] in mapping concurrent networks and spatial overlaps in the future.

In summary, our work has inferred and characterized 32 reproducible and meaningful functional networks and their spatial overlap patterns for each subject in the HCP data, forming an initial version of holistic atlases of functional networks and interactions (HAFNI). These HAFNIs revealed a new and reproducible functional architecture principle of the human cortex, that is, reciprocal localizations of HHRs and HSRs. In the future, it will be invaluable to further assess possible alterations of HAFNI components and interactions in brain disorders such as Alzheimer's disease and Schizophrenia.

Acknowledgement

T. Liu was supported by NSF CAREER Award (IIS-1149260), NIH R01 DA-033393, NIH R01 AG-042599, and NSF CBET-1302089. L Guo was supported by NSFC 61273362 and NSFC 61333017. J Lv and T Zhang were supported by the China Government Scholarship and the Doctorate Foundation of NWPU.

References

[1] Heeger DJ, and Ress D. 2002. What does fMRI tell us about neuronal activity? Nature Reviews Neuroscience. 3(2): 142-151.

[2] Fedorenko E, Duncan J, and Kanwisher N. 2013. Broad domain generality in focal regions of frontal and parietal cortex. Proceedings of the National Academy of Sciences. 110(41): 16616-16621.

[3] Fox MD, Snyder AZ, Vincent JL, Corbetta M, Van Essen DC, and Raichle ME. 2005. The human brain is intrinsically organized into dynamic, anticorrelated functional networks. Proceedings of the National Academy of Sciences of the United States of America. 102(27): 9673-9678.

[4] Dosenbach NU, Visscher KM, Palmer ED, Miezin FM, Wenger KK, Kang HC, Burgund ED, Grimes AL, Schlaggar BL and Petersen SE. 2006. A core system for the implementation of task sets. Neuron. 50(5): 799-812.

[5] Duncan J. 2010. The multiple-demand (MD) system of the primate brain: mental programs for intelligent behaviour. Trends in cognitive sciences. 14(4): 172-179.

[6] Pessoa L. 2012. Beyond brain regions: Network perspective of cognition–emotion interactions. Behavioral and Brain Sciences. 35(03): 158-159.

[7] Bullmore E and Sporns O. 2009. Complex brain networks: graph theoretical analysis of structural and functional systems. Nature Reviews Neuroscience. 10(3): 186-198.

[8] Huettel SA, Song, AW, and McCarthy G. 2004. Functional magnetic resonance imaging. Sunderland: Sinauer Associates.

[9] Kanwisher N. 2010. Functional specificity in the human brain: a window into the functional architecture of the mind. Proceedings of the National Academy of Sciences. 107(25): 11163-11170.

[10] Friston KJ, Holmes AP, Worsley KJ, Poline JP, Frith CD, and Frackowiak RS. 1994. Statistical parametric maps in functional imaging: a general linear approach. Human Brain Mapping. 2(4): 189-210.

[11] Worsley KJ. 1997. An overview and some new developments in the statistical analysis of PET and fMRI data. Human Brain Mapping. 5(4): 254-258.

[12] Logothetis NK. 2008. What we can do and what we cannot do with fMRI. Nature. 453(7197): 869-878.

[13] Krekelberg B, Boynton GM, and Van Wezel RJ. 2006. Adaptation: from single cells to BOLD signals. Trends in neurosciences. 29(5): 250-256.

[14] Anderson ML, Kinnison J, and Pessoa L. 2013. Describing functional diversity of brain regions and brain networks. NeuroImage.73: 50-58.

[15] Gazzaniga MS(Ed.). 2004. The cognitive neurosciences III. The MIT Press.

[16] Biswal BB. 2012. Resting state fMRI: a personal history. Neuroimage. 62(2): 938-944.

[17] Fox MD, and Raichle ME. 2007. Spontaneous fluctuations in brain activity observed with functional magnetic resonance imaging. Nature Reviews Neuroscience. 8(9), 700-711.

[18] Biswal BB, Kylen, JV, and Hyde JS. 1997. Simultaneous assessment of flow and BOLD signals in resting-state functional connectivity maps. NMR in Biomedicine. 10(45): 165-170.

[19] Beckmann CF, DeLuca M, Devlin JT, and Smith SM. 2005. Investigations into resting-state connectivity using independent component analysis. Philosophical Transactions of the Royal Society B: Biological Sciences. 360(1457): 1001-1013.

[20] Calhoun VD, Pekar JJ, and Pearlson GD. 2004. Alcohol intoxication effects on simulated driving: exploring alcohol-dose effects on brain activation using functional MRI. Neuropsychopharmacology. 29:2097–3017.

[21] Van den Heuvel M, Mandl R, and Pol HH. 2008. Normalized cut group clustering of resting-state FMRI data. PloS one. 3(4): e2001.

[22] Chen H, Li K, Zhu D, Zhang T, Jin C, Guo L, Li L and Liu T. 2013. Inferring Group-wise Consistent Multimodal Brain Networks via Multi-view Spectral Clustering, IEEE Transactions on Medical Imaging. In press.

[23] Biswal BB. 2011. Resting State Functional Connectivity. Biological Psychiatry. 69(9): 200S-200S.

[24] Xu, J., Potenza, M. N., & Calhoun, V. D. 2013. Spatial ICA reveals functional activity hidden from traditional fMRI GLM-based analyses. Frontiers in neuroscience, 7.

[25] Lee K, Tak S, and Ye JC. 2011. A data-driven sparse GLM for fMRI analysis using sparse dictionary learning with MDL criterion. Medical Imaging, IEEE Transactions on. 30(5):1076-1089.

[26] Daubechies I, Roussos E, Takerkart S, Benharrosh M, Golden C, D'ardenne K, Richter W, Cohen JD and Haxby J. 2009. Independent component analysis for brain fMRI does not select for independence. Proceedings of the National Academy of Sciences. 106(26): 10415-10422.

[27] Raichle ME. 2010. Two views of brain function. Trends in cognitive sciences. 14(4): 180-190.

[28] Barch DM, Burgess GC, Harms MP, Petersen SE, Schlaggar BL, Corbetta M, Glasser MF, Curtiss S, Dixit S, Feldt C, Nolan D, Bryant E, Hartley T, Footer O, Bjork JM, Poldrack R, Smith S, Johansen-Berg H, Snyder AZ, Van Essen DC. 2013. Function in the Human Connectome: Task-fMRI and Individual Differences in Behavior. NeuroImage. 80:169–189.

[29] Wright J, Yang AY, Ganesh A, Sastry SS, and Ma Y. 2009. Robust face recognition via sparse representation. Pattern Analysis and Machine Intelligence, IEEE Transactions on. 31(2): 210-227.

[30] Mairal J, Bach F, Ponce J, and Sapiro G. 2010. Online learning for matrix factorization and sparse coding. The Journal of Machine Learning Research. 11: 19-60.

[31] Smith SM, Andersson J, Auerbach EJ, Beckmann CF, Bijsterbosch J, Douaud G, Duff E, Feinberg DA, Griffanti L, Harms MP, Kelly M, Laumann T, Miller KL, Moeller S, Petersen S, Power J, Salimi-Khorshidi G, Snyder AZ, Vu AT, Woolrich MW, Xu J, Yacoub E, Uğurbil K, Van Essen DC, and Glasser MF. 2013. Resting-state fMRI in the Human Connectome Project. NeuroImage. 80(15): 144-168.

[32] Donoho DL. 2006. Compressed sensing. Information Theory, IEEE Transactions on. 52: 1289-1306.

[33] Huang K, and Aviyente S. 2006. Sparse representation for signal classification. In Advances in neural information processing systems. 609-616.

[34] Wright J, Ma Y, Mairal J, Sapiro G, Huang TS, and Yan S. 2010. Sparse representation for computer vision and pattern recognition. Proceedings of the IEEE. 98(6): 1031-1044.

[35] Yang M, Feng X, Zhang D. 2011. Fisher discrimination dictionary learning for sparse representation. In Computer Vision (ICCV), IEEE International Conference on. 543-550.

[36] Li Y, Namburi P, Yu Z, Guan C, Feng J, Gu Z. 2009. Voxel selection in FMRI data analysis based on sparse representation. IEEE Trans Biomed Eng. 56(10): 2439-2451.

[37] Li Y, Long J, He L, Lu H, Gu Z, and Sun P. 2012. A Sparse Representation-Based Algorithm for Pattern Localization in Brain Imaging Data Analysis. PLoS ONE. 7(12): e50332.

[38] Oikonomou VP, Blekas K, Astrakas L. 2012. A sparse and spatially constrained generative regression model for fMRI data analysis, IEEE Trans Biomed Eng. 59(1): 58-67.

[39] Abolghasemi V, Ferdowsi S, and Sanei S. 2013. Fast and incoherent dictionary learning algorithms with application to fMRI. Signal, Image and Video Processing. 1-12.

[40] Lee H, Battle A, Raina R, and Ng AY. 2007. Efficient sparse coding algorithms. Advances in Neural Information Processing Systems. 19: 801–808.

[41] Smith SM, Fox PT, Miller KL, Glahn DC, Fox PM, Mackay CE, Filippini N, Watkins KE, Torod R, Laird AR and Beckmann CF. 2009. Correspondence of the brain's functional architecture during activation and rest. Proceedings of the National Academy of Sciences. 106(31): 13040-13045.

[42] Raichle ME, MacLeod AM, Snyder AZ, Powers WJ, Gusnard DA, and Shulman GL. 2001. A default mode of brain function. Proceedings of the National Academy of Sciences. 98(2): 676-682.

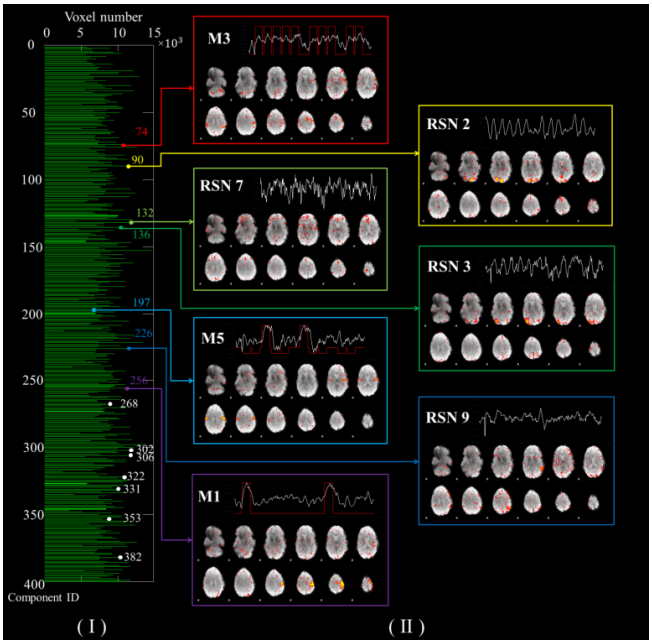

(a)

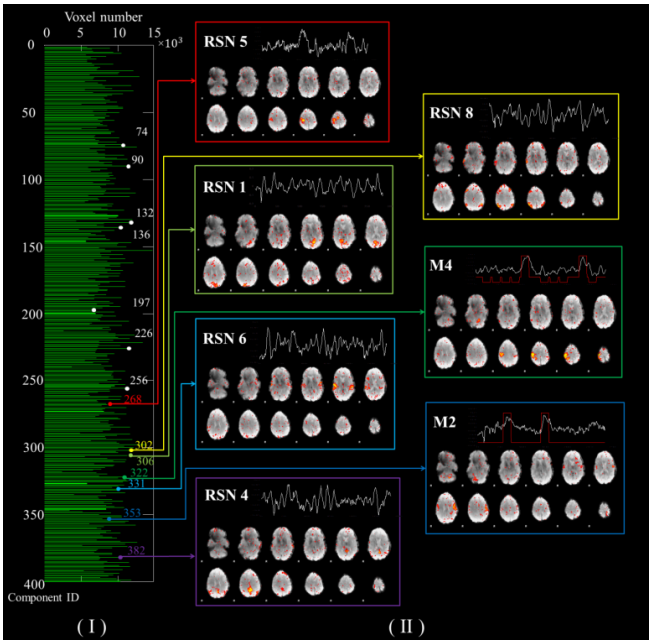

(b)

Fig. 1. The decomposed dictionary components of the motor task fMRI data of one single task (I) and the corresponding reference weight maps (14 maps shown in (II)) by applying the HAFNI method to the whole-brain fMRI signals. Figures (a) and (b) visualize 14 selected dictionary components which are either motor task-evoked networks (M1-M5) or resting state networks (RSN1-RSN9), respectively. The green bars in (I) show 400 dictionary network components (indexed vertically) and the spatial non-zero voxel numbers that each component's reference weight map contains (represented by the horizontal height). The panels in (II) visualize the temporal time series (white curve) and spatial distribution map (eight representative volume images) of each network. The red curves represent the task contrast designs of the motor tfMRI data.

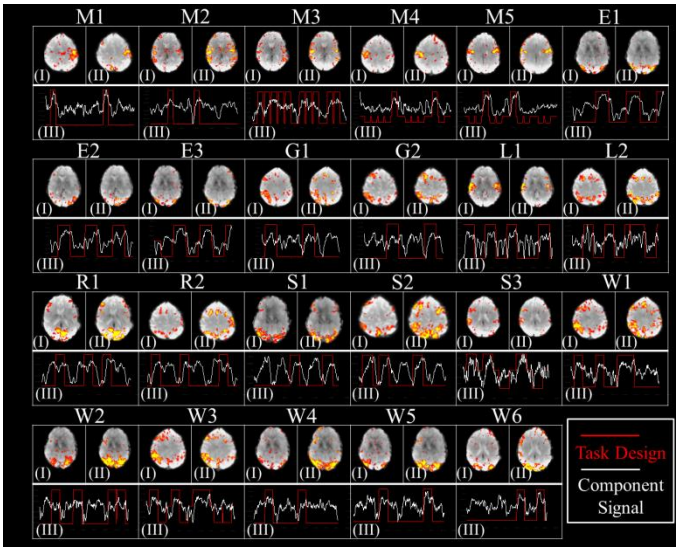

(a)

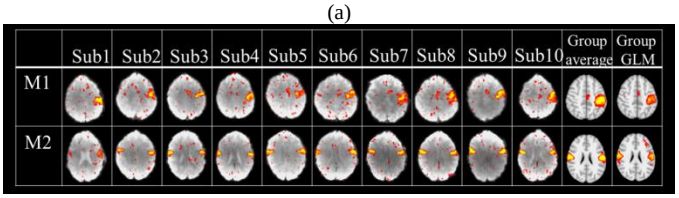

(b)

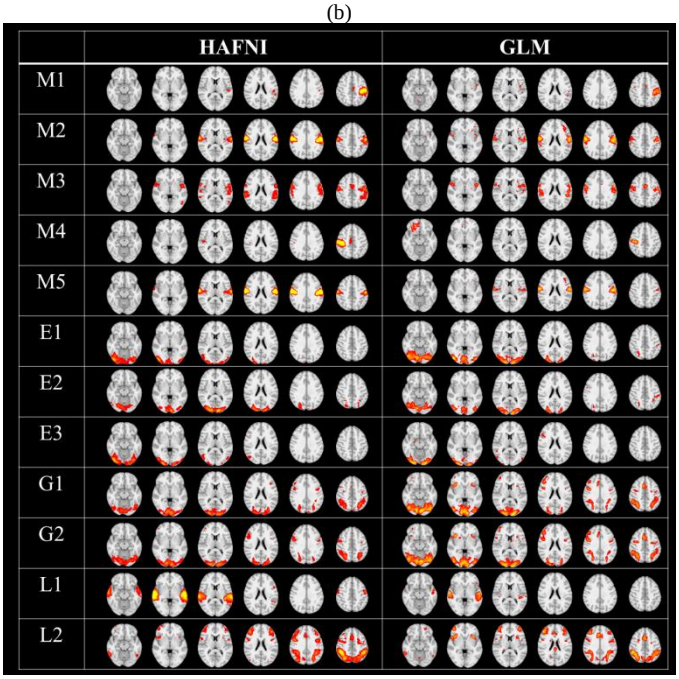

(c)

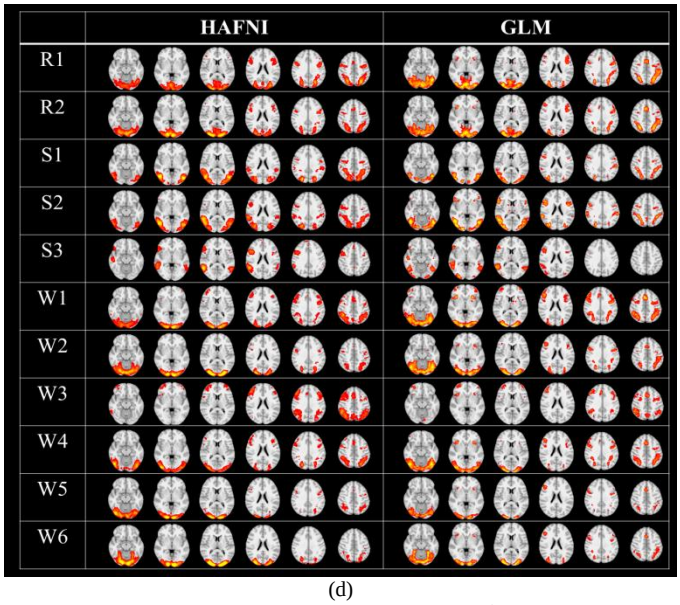

(d)

Fig. 2. The task-evoked HAFNI components in seven tfMRI datasets and the comparison with GLM-derived activation maps. Seven tasks are language network (L), motor network (M), gambling network (G), emotion network (E), social network (S), relational network (R) and working memory network (WM). (a) Examples of 23 task-evoked HAFNI components in seven tasks in one subject. Each panel includes one HAFNI component and has three sub-figures (I-III). (I) One representative slice from a HAFNI component's spatial reference weight map. (II) The corresponding representative slice of the activation map by GLM. (III) The comparison of task paradigm curve and the HAFNI component's temporal time series. (b) Examples of group-wise consistency of the HAFNI component's spatial reference weight maps across different HCP subjects (10 subjects shown here). Two HAFNI components in the motor task are shown. The last two columns are the group-wise averages of HAFNI components and the group-wise GLM activation maps. (c) Group-wise averages of 12 identified HAFNI components across 68 HCP subjects for the four tasks as well as the corresponding averaged GLM-derived activation maps (right column). Six representative volume slices were selected for visualization for each component. (d) Group-wise averages of 11 other identified HAFNI components across HCP subjects for the three tasks, as well as the corresponding averaged GLM-derived activation maps (right column). Similarly, six representative volume slices were selected for visualization for each component.

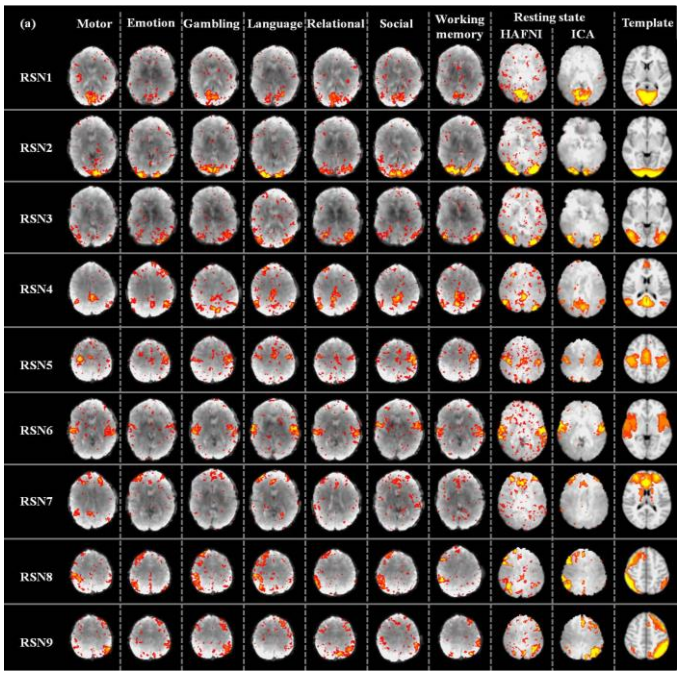

(a)

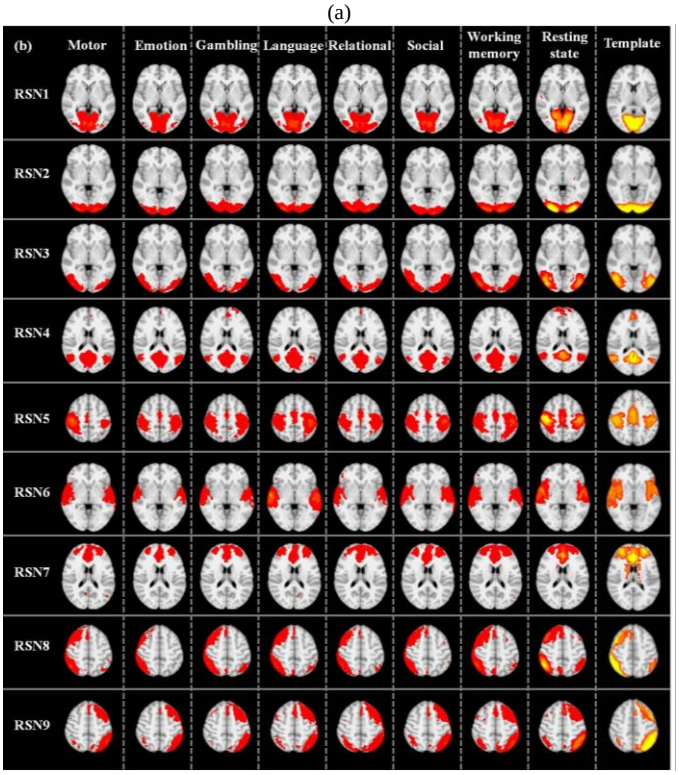

(b)

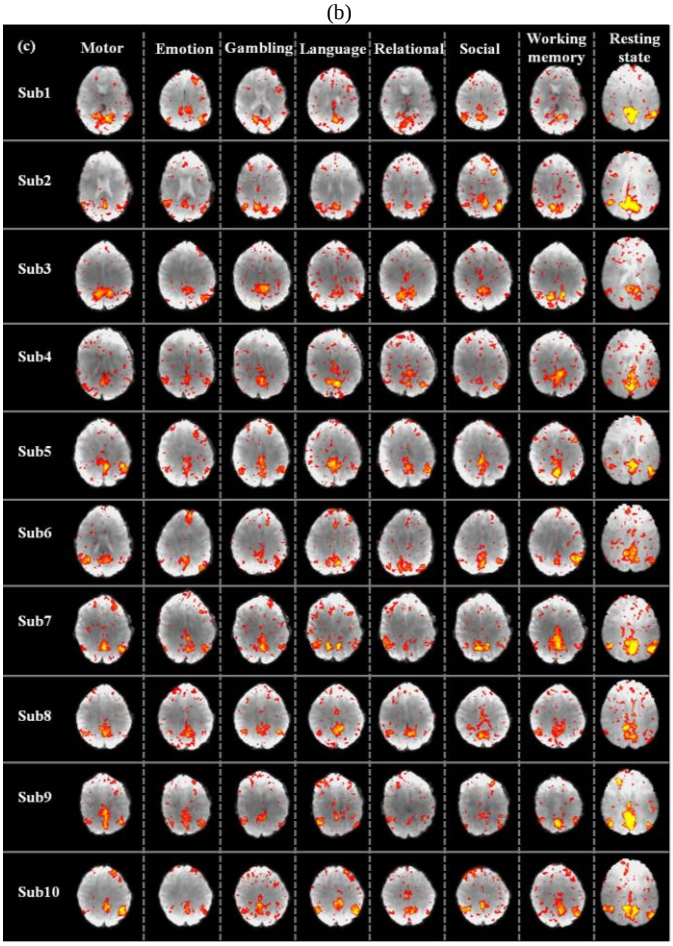

(c)

Fig. 3. The nine HAFNI RSNs identified from seven tfMRI datasets and one rsfMRI dataset and their comparisons with corresponding ICA-derived components. (a) Examples of 9 HAFNI RSNs (nine rows) in seven tfMRI datasets (the first seven columns) in one subject. The eighth column shows the

HAFNI RSNs derived from rsfMRI data and the ninth columns show the corresponding ICA-derived components. The last column shows the corresponding RSN templates. For each RSN template, the representative slice, which is superimposed on the MNI152 template image and thresholded at z=3, is shown as the spatial pattern of the specific RSN. For the spatial maps of identified RSNs via HAFNI or ICA, the most informative slice superimposed on the mean fMRI image of each subject is shown. The color scale of spatial maps of HAFNI RSNs ranges from 0.1 to 10. The ICA spatial maps were converted to and shown as the Z-transformed statistic maps using the default threshold value of 0.5. (b) The group-wise averaged HAFNI RSNs in all seven tfMRI and one rsfMRI datasets. In each sub-figure, the most informative slice, which is superimposed on the MNI152 template image, is shown as the spatial pattern of a specific RSN. The color scale of the spatial maps of identified RSNs ranges from 0.5 to 10 in rsfMRI data, and is 0.2 to 10 in other seven tfMRI data. (c) Examples of HAFNI RSN #4 (DMN) in seven tfMRI and one rsfMRI datasets of 10 randomly selected HCP subjects.

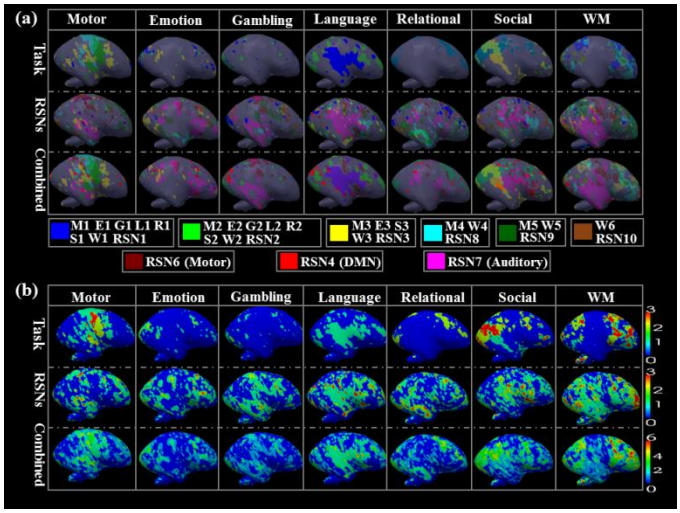

Fig. 4. Illustration of the spatial overlap patterns among task-evoked HAFNIs and HAFNI RSNs. (a) showed the overlaps of task-evoked HAFNI components and HAFNI RSNs of the same subject. The first row displayed the overlaps of multiple contrast-evoked components within seven tasks. The second row showed the overlaps of nine HAFNI RSNs. The third row overlapped different contrast-evoked HAFNI components (the first row) and three HAFNI RSNs (DMN, motor and auditory networks) together. Networks are represented with different colors as noted in the bottom color tables in (a). (b) Maps of the numbers of HAFNI components that each cortical region is involved in for the corresponding brains in (a). Each row and each column are in correspondences with (a). The numbers of involved HAFNI components are color-coded according to the color bar in each row.

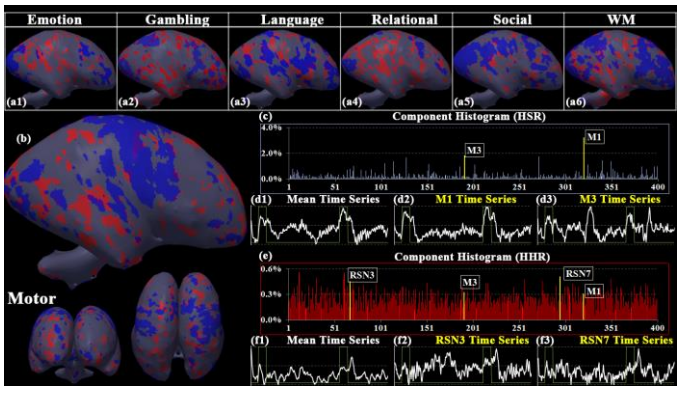

Fig. 5. Illustration of the spatial and temporal characteristics of the HHR and HSR of a randomly-selected subject. In (a1-a6), we visualized HHR (red) and HSR (blue) on the inflated cortical surface in 6 tasks. In addition, we have provided three views of the HHR (red) and HSR (blue) in (b) obtained from the motor task. The lateral view is zoomed to show more details. It should be noted that in each task, regions visualized as HSR are the union of multiple HSRs corresponding to each task contrast map from that task. For example, the visualization of the "Emotion" HSR on the surface is the union of the GLM-derived activation maps from both of the "Faces-Baseline" and "Shapes-Baseline" contrasts. The temporal characteristics of a specific HSR picked from multiple contrast maps of the motor task are summarized in (c) by the overall component composition (histogram) of that region. The mean fMRI time series of the same HSR is shown in (d1), and mean fMRI time series of the two HAFNI component M1 and M3 in the motor task are shown in d2 and d3. It should be noted that M1 and M3 are two dominant components in the overall composition histogram. Similarly, the component histogram of HHR in the motor task is shown in (e), with the mean fMRI time series of HHR shown in (f1). The mean fMRI time series of two HAFNI RSNs: RSN3 and RSN7, which have relatively high percentages in the component histogram of HHR, are also shown here.

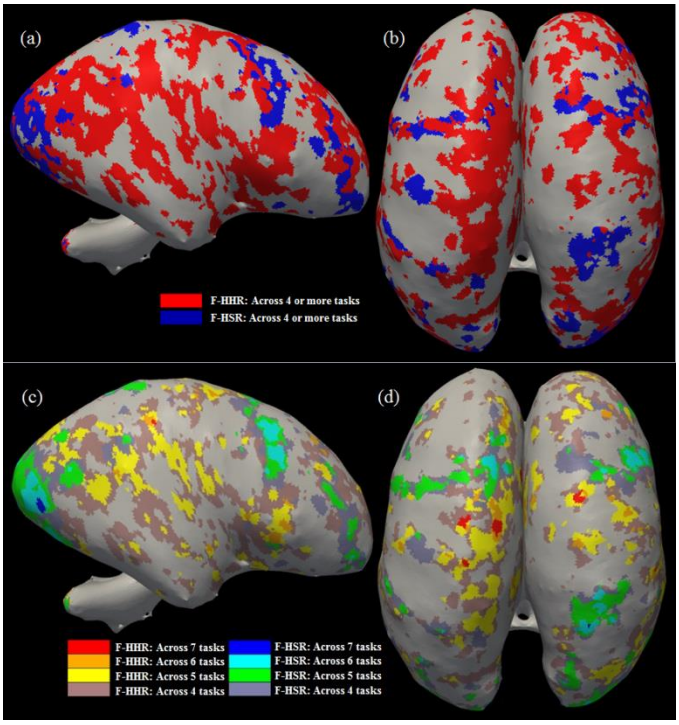

Fig. 6. Visualization of the frequent HHRs (F-HHR) and frequent HSRs (F-HSR) for one individual brain (the same subject in Fig.5.) across 7 tasks. Here, if an HHR or HSR region appears at least 4 times across 7 tasks (any possible combination from 7 tasks), it is considered as an F-HHR or F-HSR. (a)-(b): Joint distributions of F-HHRs and F-HSRs on the inflated cortical surface color-coded according to the color bar at the bottom. For example, the red color indicates that the corresponding cortical area has been identified as F-HHR in at least 4 tasks. Meanwhile, the F-HSRs that appear at least 4 times across 7 tasks are visualized as blue regions on the surface. Figures (a) and (b) are two perspective views of the same subject. (c)-(d): Joint distributions of F-HHRs and F-HSRs that are common across 4, 5, 6 and 7 tasks (any possible combination from 7 tasks), respectively, on the inflated cortical surface color-coded according to the color bar at the bottom. For example, the red color indicates that the corresponding cortical area has been identified as F-HHR in all 7 tasks. Meanwhile, the F-HSRs that appear across all 7 tasks are visualized as blue regions on the surface. Figures (c) and (d) show two perspective views of the same subject.